rf and thermal design studies of a 704.4 MHz, $\beta \approx 0.2$, continuous-wave rf quadrupole accelerator for frequency jump

Bowen Zhou*

Department of Physics, Nanjing University, 642000 Nanjing, China; GSI Helmholtzzentrum für Schwerionenforschung, 64291 Darmstadt, Planckstraße 1, Germany; and Suzhou Laboratory, 215000 Suzhou, China

Chuan Zhang†

GSI Helmholtzzentrum für Schwerionenforschung, 64291 Darmstadt, Planckstraße 1, Germany; Institute for Applied Physics, Goethe-University, 60438 Frankfurt am Main, Germany; and Helmholtz Research Academy Hesse for FAIR (HFHF), 60438 Frankfurt am Main, Germany

(Received 22 October 2023; accepted 29 January 2024; published 27 February 2024)

The radio-frequency quadrupole (RFQ) linac is often used as the first radio-frequency (rf) structure for both bunching and preaccelerating proton or heavy ion beams directly behind an ion source or a low-energy beam transport section. Typically, RFQ linacs operate at frequencies below 450 MHz and beam velocity ranges from $\beta = 0.01$–0.08. Taking the MYRRHA project as an example, a 704.4 MHz continuous-wave (cw) RFQ linac has been recently proposed to realize an efficient fourfold frequency jump at $\beta \approx 0.2$. Due to its high frequency, small dimensions, and cw operation mode, careful design studies for the RFQ cavity structure including the water-cooling channels have been further performed, integrating the idea of using additive manufacturing technology for future construction. Systematic rf and thermal simulations and analysis demonstrated the reliability of the 704.4 MHz RFQ linac at cw operation and the frequency tuning ability via water-speed adjustments. This investigation shows that it could be a highly promising solution to perform an efficient frequency jump with a high-frequency RFQ accelerator at $\beta \approx 0.2$ for large-scale hadron linacs, which could potentially shorten the low- and medium-β parts of the whole facility.

DOI: 10.1103/PhysRevAccelBeams.27.020101

I. INTRODUCTION

In large-scale hadron linear accelerators, it is a common practice to perform frequency jumps with the increase of beam energy [1–4]. In the low-energy section, low-frequency linacs are preferred, because lower-frequency radio-frequency quadrupole (RFQ) linacs have higher shunt impedance and a reasonable accelerating cell length could be obtained. While in the high-energy section, high-frequency accelerating structures could keep the whole linac compact so that the construction and operation costs can be significantly reduced. However, the transition from the low frequency to the high frequency (the frequency jump) would result in the multiplication of the longitudinal bunch length in degrees. Therefore, it is important to have a proper rebunching in the frequency jump section to reduce the bunch length and fit the beam into the longitudinal acceptance of higher-frequency rf cavities. To avoid the beam loss and emittance growths, the frequency jump transition is typically chosen in the medium-β range $0.4 < \beta < 0.6$ [1–4], as space charge effects are most pronounced in the low-β range.

Taking the MYRRHA project [5] as an example, a previous study [6] proposed two new frequency jump solutions at $\beta \approx 0.2$, one so-called RFQ-based solution (using a combination of a 704.4 MHz RFQ and a 704.4 MHz CH cavity [7]) and one so-called CH-only solution (using four 704.4 MHz CH cavities). Systematic beam dynamics simulations and error analysis demonstrated that both solutions can achieve an efficient fourfold frequency jump from 176.1 to 704.4 MHz with almost no beam loss, whereas the RFQ-based solution would be more favorable due to its robustness against errors and ease of water cooling. Figure 1 shows the usage of the proposed frequency jump RFQ for large-scale hadron linacs schematically (using MYRRHA as an example). For the 704.4 MHz CH structure, follow-up studies have been further performed [7,8]. This paper will focus on the rf and thermal design studies of the 704.4 MHz frequency jump RFQ (hereafter referred to as the FJ RFQ), and the main

*Zhoubw@szlab.ac.cn
†C.Zhang@gsi.de

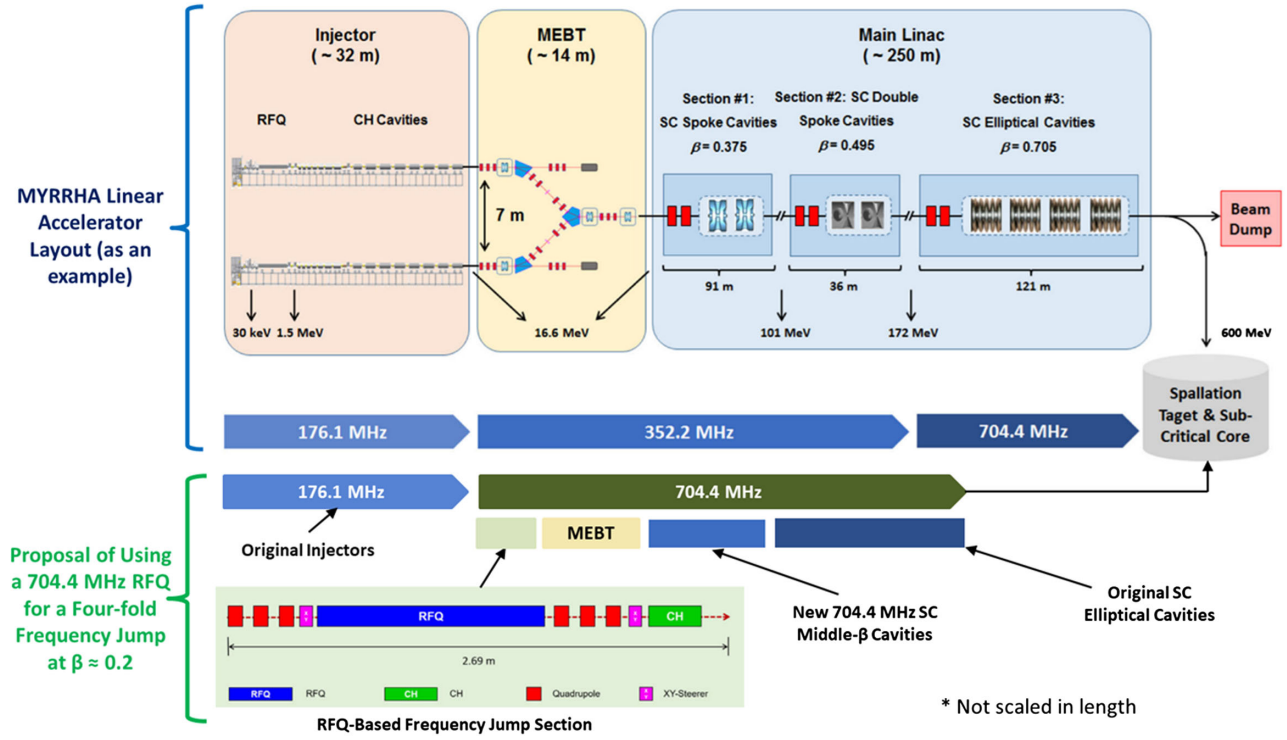

FIG. 1. An overview sketch showing the usage of the proposed frequency jump RFQ for large-scale hadron linacs (using MYRRHA as an example). The MYRRHA accelerator design adopts twice double frequency jumps, whereas the new solution only uses one fourfold frequency jump, increasing the frequency directly from 176.1 to 704.4 MHz by an RFQ-based frequency jump section [6].

design parameters of the FJ RFQ [6] can be found in Table I. The FJ RFQ covers a beam-energy range from 16.6 to 16.8 MeV, corresponding to $\beta \approx 0.2$. Since it is mainly used for bunching, acceleration is not the task. In view of RFQ injectors, the average beam energy of the FJ RFQ is one order higher than normal RFQ linacs. While in the view of rf structures for the frequency jump, the FJ RFQ operates at relatively low energy, compared to the typical frequency jump transition velocities of $0.4 < \beta < 0.6$.

TABLE I. Some important beam properties and structure parameters of the FJ RFQ and the CERN 750 MHz RFQ linacs (PIXE and HF-RFQ).

Parameters	FJ RFQ	PIXE	HF-RFQ
RFQ type	4 vane	4 vane	4 vane
Ion species	Proton	Proton	Proton
Frequency f (MHz)	704.4	750	750
Input energy W_{in} (MeV)	16.6	0.02	0.04
Output energy W_{out} (MeV)	16.8	2.0	5.0
Peak beam current I (mA)	5	2×10^{-4}	0.1
Transport efficiency (%)	100	30	30
Inter-vane voltage V (kV)	31	35	68
Duty cycle (%)	100	2.5	0.4
Kilpatrick factor	0.15	1.44	2
Vane tip transverse radius R_v (mm)	19.8	1.439	1.5
Aperture radius r_0 (mm)	15.9	0.706	2
Vane length L (m)	1.23	1.073	2

Traditionally, normal conducting accelerator cavities are fabricated in parts by machining and then joined together by brazing or welding. Additive manufacturing (AM) technology is a kind of state-of-the-art technology for accelerator construction, which enables the production of complicated metal components using laser or electron beams to scan a metal-powder bed layer by layer according to the 3D CAD slice model. It has been shown that the AM technology is especially suitable for the construction of high-frequency accelerators that have small radial dimensions and complicated cooling channels [8]. Now there is an increasing interest in realizing different types of linear accelerators using the AM technology [9], for example, the 4-vane type RFQ [10,11], the CH-type DTL [8], the IH-type DTL [12,13], and the quarter wave resonator [14]. Recent investigations in CERN studied the geometric accuracy and surface roughness of a 750 MHz 4-vane type RFQ linac made by laser powder bed fusion, it showed that the surface precision of the AM-made RFQ is approaching the required precision of 20 μm on the vane tip and fully reaching 100 μm on other surfaces even without surface finishing operations [10,11]. The required surface roughness $R_a < 0.4$ μm can be accomplished by three different postprocessing methods. The study confirmed the feasibility of using pure-copper AM printing for the construction of high-frequency RFQ linacs.

A comparison of the main design parameters between the FJ RFQ and the other two > 700 MHz RFQ linacs (the

750 MHz HF-RFQ [15–18], and PIXE RFQ [19,20]) can be found in Table I. Although the three RFQ linacs are all 4-vane machines and have similar operation frequencies, they are fairly different as follows:

(i) The 750 MHz RFQs (almost all RFQ linacs) are mainly for acceleration at $\beta < 0.1$, while the FJ RFQ is mainly for bunching at $\beta \approx 0.2$. As a result, the unit cell length ($\beta\lambda/2$) of the FJ RFQ is much larger than the 750 MHz RFQ linacs. Additionally, the vane tip radius and aperture radius of the FJ RFQ are also much larger, which allows the FJ RFQ to have a larger tolerance to the manufacturing errors caused by the AM technology.

(ii) The FJ RFQ has been designed for bunching a relatively high-intensity cw proton beam with 100% beam transmission efficiency. The beam current, duty cycle, and beam transmission efficiency of the FJ RFQ linacs are all much higher than the two 750 MHz RFQ linacs. The cw operation of the FJ RFQ requires that more attention should be paid to the thermal deformation and frequency detuning problems. Fortunately, the AM technology provides the convenience of producing specific-shaped quadrants to improve the intrinsic quality factor and dedicated water-cooling channels to enhance the cooling effect. Subsequent sections will present detailed rf and thermal design studies to ensure a safe and reliable cw operation of the FJ RFQ.

II. RADIO FREQUENCY DESIGN AND STRUCTURE OPTIMIZATION

A. The optimal quadrant shape

The lumped circuit model of a four-vane RFQ, as illustrated in Fig. 2, provides insights into the dependencies of the rf parameters from the geometry. In Fig. 2, C represents the capacitance, and L represents the inductance per vane length within one quadrant. Given that the magnetic flux in each quadrant is uniform, the inductance can be expressed as $L = \mu_0 A$, where μ_0 is the permeability of free space, and A represents the area of each quadrant. The RFQ resonant frequency can be expressed as

$$\omega = (LC)^{-1/2} = (\mu_0 AC)^{-1/2}. \tag{1}$$

Since the capacitance per unit length has a weak function of the vane shape [21], the resonant frequency is only dependent on the quadrant area A, which means for an RFQ with one certain frequency the quadrant area is approximated to a constant. Given the voltage on each vane tip is $\pm V e^{j\omega t}/2$, the surface current flowing on each quadrant per unit length should be

$$I = C\frac{\mathrm{d}V}{\mathrm{d}t} = j\omega CV e^{j\omega t}. \tag{2}$$

Substituting Eqs. (1) and (2) into the expression of the power dissipation per unit length $P = R_s|I|^2 C_r/2$, where

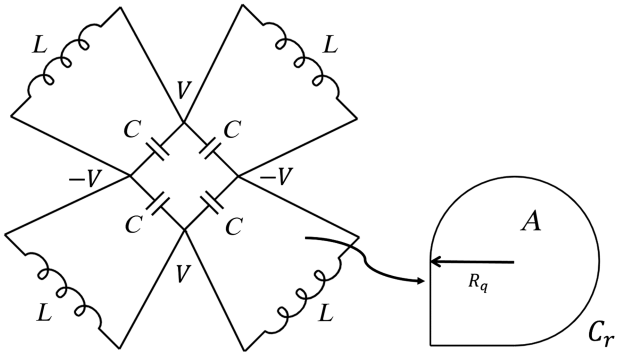

FIG. 2. Equivalent lumped circuit of the quadrupole mode of a four-vane RFQ, and the idealized quadrant shape with area A and circumference C_r.

R_s $(= \sqrt{\mu_0\omega/2\sigma})$ is the surface resistance, C_r is the circumference of the cross section of each quadrant, and σ is the copper conductivity, it is obtained that

$$P = C_r\sqrt{\frac{\mu_0}{8\sigma}}\omega^{5/2}C^2V^2. \tag{3}$$

As the stored energy per length in each quadrant $U = CV^2/2$, the intrinsic quality factor can be derived as

$$Q_0 = \frac{\omega U}{P} = \frac{1}{C_r C\omega^{3/2}}\sqrt{\frac{2\sigma}{\mu_0}}, \tag{4}$$

which demonstrates that the intrinsic quality factor is inversely proportional to the quadrant's circumference C_r. Improving the intrinsic quality factor of an RFQ linac with a fixed frequency means reducing the quadrant circumference while keeping the area of each quadrant unchanged. Therefore, the quadrant shape is intended to be circular for a high shunt impedance.

B. Detailed rf structure design

The front view of a simplified 704.4 MHz RFQ structure has been presented [6], where the aperture radius r_0 and the vane radius R_v are predefined based on the beam dynamics design. Nevertheless, it is a preliminary design of the RFQ cavity with simplified water-cooling channels for checking the basic rf and thermal performance, without any insert port and rf structure optimization. Through the investigation of the lumped-circuits model, we know that the intrinsic quality factor is inversely proportional to the quadrant's circumference C_r, which implies that the intrinsic quality factor will increase as the quadrant shape approaches a circle. The circular-shaped quadrants were seldom adopted in the existing RFQ linacs due to the challenges in manufacturing and brazing, but the advancements in AM technology make the four quadrants feasible to be produced as a whole.

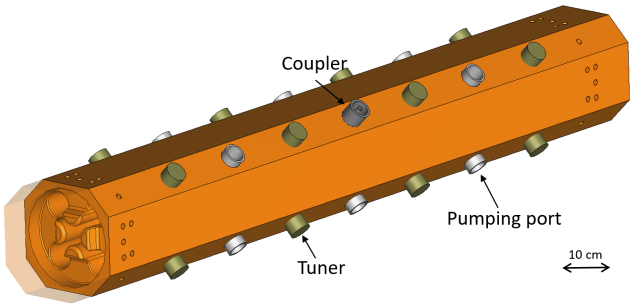

FIG. 3. 3D model of the FJ RFQ, 1 power coupler, 16 tuners, and 11 pumping ports are reserved.

The three-dimensional design for the FJ RFQ with circular-shaped quadrants is depicted in Fig. 3. In the design of the RFQ, ports for the power coupler, 16 tuners, and 11 vacuum pumps have been reserved. The dimensions of the circular-shaped quadrant are labeled in Fig. 4. From the eigenmode simulation by CST MWS [22], it is obtained that as the total stored electromagnetic energy inside the RFQ cavity is 1 J, the rf power consumption is 471.4 kW, the intervane voltage is 132.6 kV, and the quality factor $Q = 9422$. As the required intervane voltage for the FJ RFQ is $U = 31$ kV, the corresponding rf power consumption $P_c = (31/132.6)^2 \times 471.4 \approx 25.8$ kW. The shunt impedance of the optimized RFQ cavity is $R_P = U^2 L/P_c \approx 45.8\ \mathrm{k\Omega \cdot m}$, which is about 7.0% higher than the shunt impedance value of $42.8\ \mathrm{k\Omega \cdot m}$ presented in the previous design [6]. Since the power coupler and other ports were not included before, the net increase of the shunt impedance should be even larger. The above rf parameters obtained from the CST MWS simulation are concluded in Table II.

Figure 5 illustrates that the TE_{210} mode resonant frequency can be adjusted continuously by changing the depth of the tuners inside the RFQ cavity, with a tuning rate of ~1 MHz/mm. Because the thermal deformation would cause the frequency rise of tens of kHz when the FJ RFQ is in high power operation (will be introduced in the next section). The frequency of the TE_{210} mode is determined at 704.34 MHz, which corresponds to the tuner depth $d_t = 8.6$ mm.

TABLE II. Eigenmode simulation results of the FJ RFQ by CST Microwave Studio.

Parameters	Value
TE_{210} mode frequency f	704.34 MHz
Frequency interval Δf	>10 MHz
Frequency tuning rate	~1 MHz/mm
RF power consumption P_c	25.8 kW
Quality factor Q	9422
Shunt impedance R_p	$45.8\ \mathrm{k\Omega \cdot m}$
Maximum E-field $E_{\max}$	3.7 MV/m
Kilpatric factor	0.15
Field flatness	±2%

The mode spectrum of the FJ RFQ against a longitudinal-mode number is shown in Fig. 6. The frequency of the TE_{210} mode is 704.34 MHz, and its nearest modes are the TE_{111} mode (694.3 MHz) and the TE_{211} mode (714.9 MHz). Sufficient safety margins (> 10 MHz) are reserved for the operating mode. As a result, the dipole stabilization rods [23] are not needed to increase the mode interval for the FJ RFQ.

C. Electromagnetic field evaluation

As well known, the rate of vacuum breakdown is influenced by the maximum strength of the electromagnetic field inside rf cavities, especially for the cw

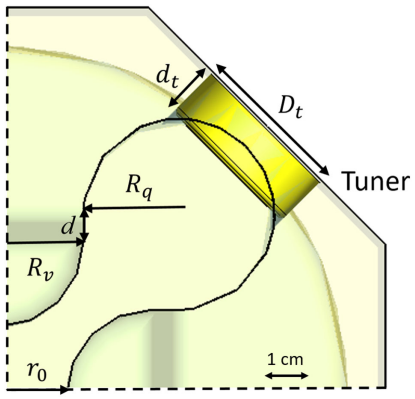

FIG. 4. Dimensions of the cross section of the circular-shaped quadrant, where the aperture radius $r_0 = 15.9$ mm, the vane radius $R_v = 19.8$ mm, the quadrant radius $R_q = 22.23$ mm, the distance from the vane center to the quadrant center $d = 6.33$ mm, and the tuner diameter $d_t = 36$ mm.

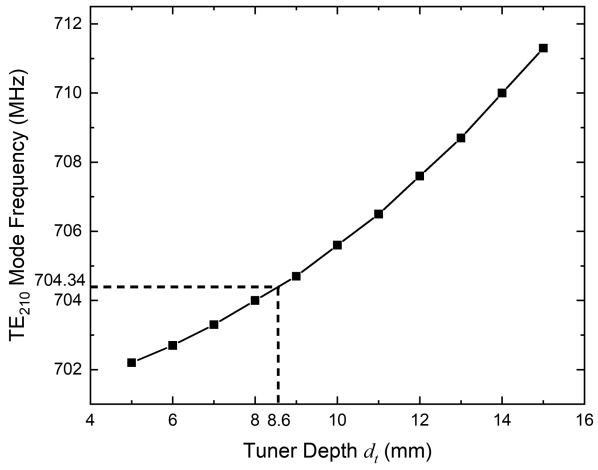

FIG. 5. Variation of the TE_{210} mode frequency with tuner depth. When the tuner depth is 8.6 mm, the resonant frequency is 704.34 MHz.

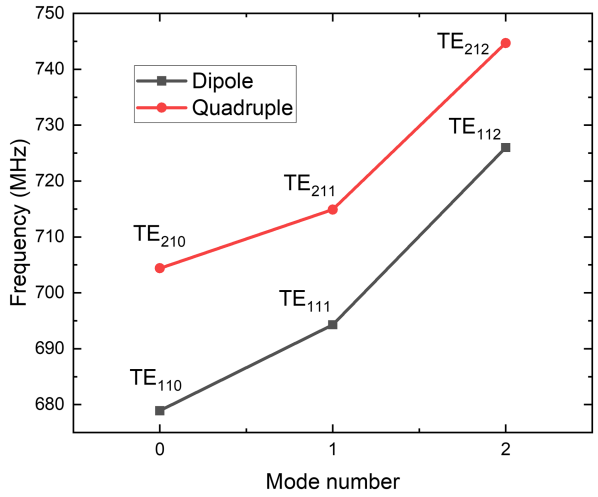

FIG. 6. Mode spectrum of the FJ RFQ against a longitudinal-mode number. The operating mode TE_{210}-like mode is working on 704.34 MHz, its most adjacent modes are the TE_{211} mode on 714.9 MHz and the TE_{111} mode on 694.3 MHz.

operation mode. Figure 7 shows the *E*-field distribution on different transverse planes, the left picture shows the *E*-field distribution in the middle of the RFQ cavity, and the right picture points out that the maximum *E*-field (∼15.8 MV/m) appears at the margins of the undercut. It should be noted that the maximum *E*-field strength of 15.8 MV/m corresponds to the intervane voltage of 132.6 kV. So as the intervane voltage is 31 kV, the maximum *E*-field strength is about 3.7 MV/m, corresponding to a Kilpatrick factor of 0.15 (the Kilpatrick limit at 704.4 MHz is 24.6 MV/m). The low Kilpatrick factor keeps the FJ RFQ away from electrical breakdown in case the surface roughness degenerates due to the AM technology.

Typically, the TE_{210} mode cannot exist in normal rf cavities, because the longitudinal magnetic field must drop to zero at the two ends. However, with the introduction of undercuts at the vane ends, the magnetic flux from each quadrant splits in half, each half flows around the undercuts, and returns to the adjacent quadrants [21]. Undercuts with smooth edges are designed in our case to minimize rf heating caused by the magnetic flux. Figure 8 depicts the normalized TE_{210}-like mode magnetic field distribution, where the small bump in the center of the distribution curve is probably induced by the input power coupler in the first quadrant. Despite variations in the field distributions, the field flatness is always within ±2%, which is a reasonable value [24,25] and could be further improved by fine-tuning with according tuners.

As well known, the surface current induced by the magnetic field inside the RFQ surfaces will cause lots of rf power dissipation and noticeable local temperature rise in particular regions. If the cooling water cannot lower the copper temperature of those regions effectively and timely, thermal expansions would cause the RFQ frequency shift or even damage to the surface in terms of microscopic cracks and roughening [26]. The distribution of surface current density in critical regions, as shown in Fig. 9, indicates that the areas most likely to experience temperature rise are around the undercuts and certain insert pieces. It is essential to prioritize effective water-cooling channels in these areas to prevent inhomogeneous heating. The related thermal analysis will be presented in the next section.

III. MULTIPHYSICS FIELD SIMULATIONS AND THERMAL ANALYSIS

A. Water-cooling channels design

It has been estimated that the average temperature rise of the FJ RFQ in the cw operation mode is about 1 K at 6 bars water pressure [6]. However, it is worth noting that local temperature rise in particular areas could be much higher than the average value. To address the issue of inhomogeneous heating, we investigate efficient water-cooling

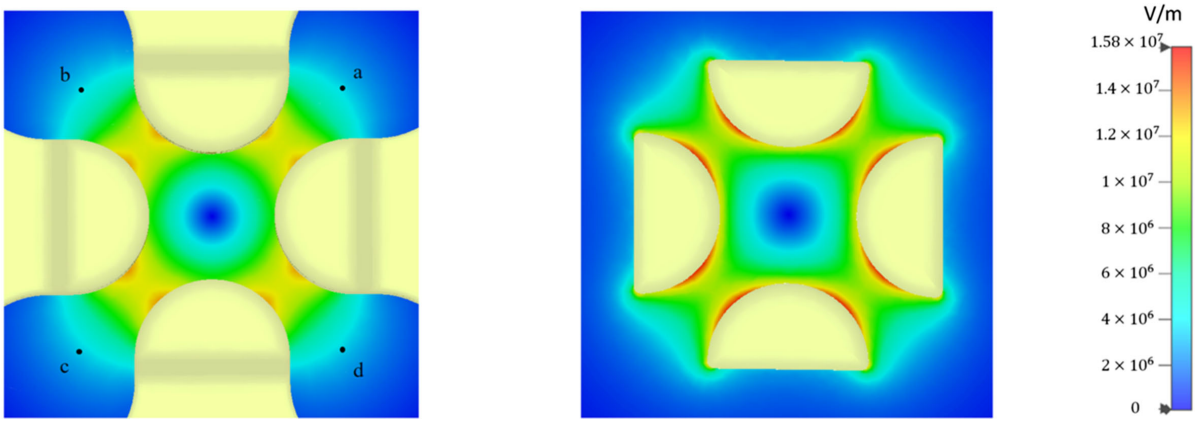

FIG. 7. *E*-field distribution on the cross sections of the FJ RFQ by CST MWS simulation, on the middle of the cavity (left), around the undercut (right), noting that the stored energy inside the RFQ cavity is 1 J in by default.

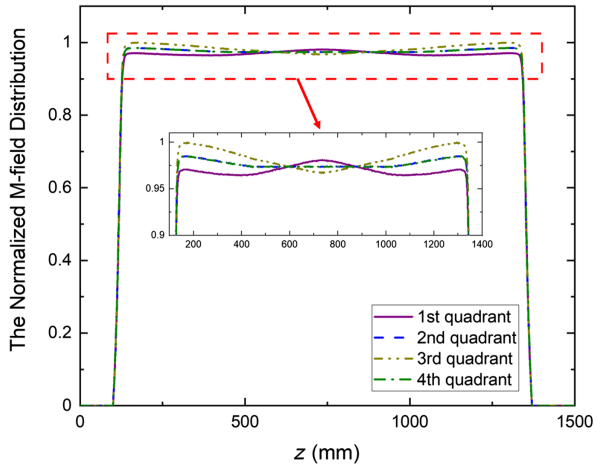

FIG. 8. Normalized magnetic field strength distribution along the beam direction in four quadrants (along a, b, c, and d four points in Fig. 7).

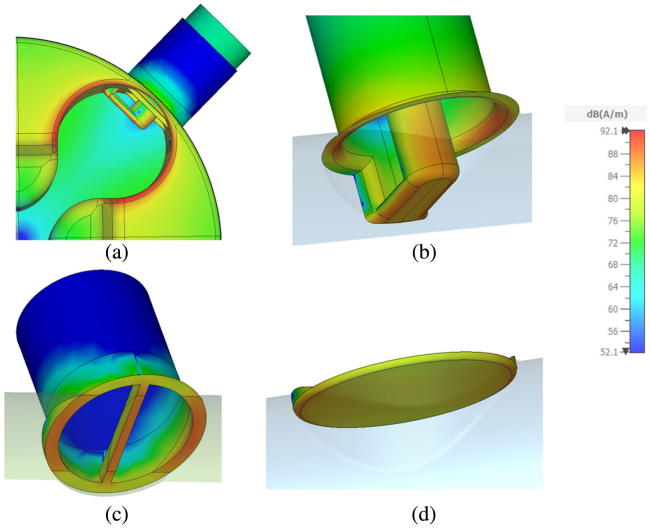

FIG. 9. Surface current density distribution inside the RFQ cavity simulated by CST MWS, as the nominal stored energy is 1 J, around (a) the undercut of one quadrant, (b) the power coupler, (c) the pumping port, and (d) the tuner.

strategies with the help of multiphysics field simulations. Dedicated water-cooling channels are designed to mitigate the inhomogeneous heating problem. The AM technology can enable complicated water-cooling channels inside the vanes, rather than only straight lines by traditional manufacturing [8]. Focused on the most dangerous areas with high surface current, curved water-cooling channels are implemented close enough to the undercut edges, and circular channels are strategically placed around the tuners, the pumping ports, and the power coupler, as depicted in Fig. 10, to enhance the cooling effect.

The steady-state thermal simulations are conducted by CST Thermal and Mechanics module, which helps to unveil the intricate temperature distribution encompassing the high surface current areas. Some important parameters obtained from the thermal simulation are listed in Table III, where 80% of the simulated shunt impedance is used to evaluate the total rf power consumption ($25.8/0.8 = 32.3$ kW), and the ambient temperature is assumed as 293 K. For 10 mm diameter channels with a water flow speed of 2 m/s, the heat convection coefficient between the cooling water and surrounding copper is about 7000 $W/m^2/K$, the heat convection coefficient between the RFQ outside surface and the ambient air is only about 10 $W/m^2/K$, which is insignificant compared to the water cooling effect [27]. The insight views of the temperature distribution around particular areas are presented in Fig. 11, the simulation points out that the most significant temperature rise (~12 K), as shown in Figs. 11(b) and 11(c), are located at the tips of the power coupler and the pumping ports. The notable temperature rise could be attributed to the high surface current intensity and the inefficiency of heat transfer into the surroundings. Since the threshold temperature rise for damage caused by the rf heating is usually quoted between 40 K and 110 K for annealed copper [26,28], the 12 K temperature rise is well acceptable.

In the next step, the temperature distribution serves as input field data for the subsequent mechanical displacement simulation. The comprehensive deformation of the entire cavity triggered by temperature rises is portrayed in Fig. 12.

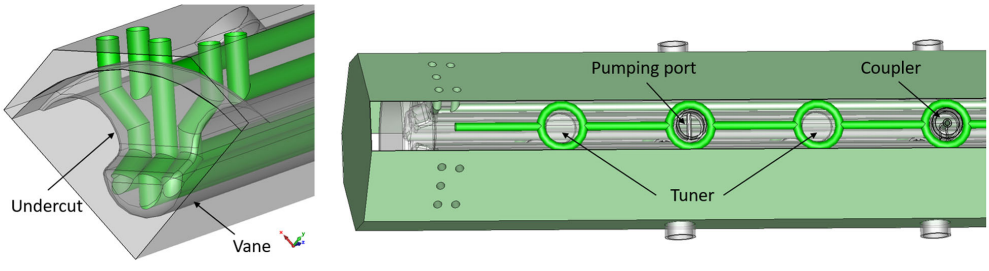

FIG. 10. Insight views at the water-cooling channels (green pipes) inside the RFQ cavity, (a) curved pipes inside one of the vanes, (b) circular pipes around the tuners, pumping ports, and power coupler.

TABLE III. Thermal simulation results of the FJ RFQ.

Parameters	Value
rf power consumption P	32.3 kW (80% of R_p)
Water flow speed v	2 m/s
Water pipe diameter d_p	10 mm
Ambient temperature T_0	293 K
Heat convection rate h	7000 (to water), 10 (to air)
Maximum temperature rise ΔT_m	12 K
Maximum thermal deformation ΔD_m	15.7 μm
Frequency detuning δf	38.1 kHz

The maximum thermal deformation (∼15.7 μm) occurs at the vane ends. The deformed RFQ structure is then taken back into the eigenmode simulation, which reveals that the detuning of the TE_{210} mode frequency is about 38.1 kHz. It implies that the designing frequency should be slightly less than 704.4 MHz, in this case when the FJ RFQ is on full-power operation, the operation frequency could be close to 704.4 MHz and fine-tuned via adjusting the speed of cooling water.

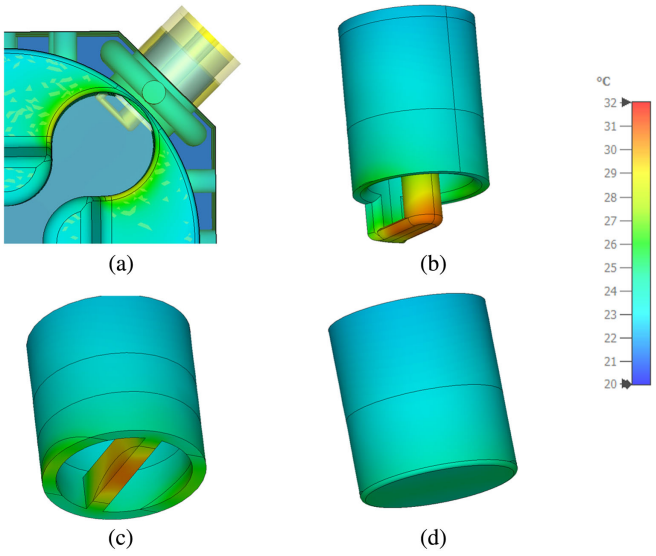

FIG. 11. Temperature rise caused by rf power loss around (a) the undercut, (b) the power coupler, (c) the pumping port, and (d) the tuner, as the ambient temperature is 20 °C.

Attributing to a possibly lower electrical conductivity and inferior surface roughness [29], the quality factor of an additive-manufactured copper cavity could be lower than the traditional-manufactured one. Therefore, additional rf power would be dissipated on the RFQ cavity to reach the required vane voltage. Figure 13 illustrates the variation of the maximum temperature rises with the increasing rf power consumption. It can be seen that even when the rf power consumption is as high as 100 kW (≈3 times the required value), the maximum temperature rise within the cavity is still below 40 K, which keeps the FJ RFQ cavity away from overheating damage. In other words, it is possible to apply higher intervane voltage in the FJ RFQ for improving the longitudinal bunching and transverse focusing effects, which allows the usage of an only-RFQ frequency jump solution to replace the RFQ-based frequency jump solution, where the 704.4 MHz CH cavity can be omitted.

B. Frequency tuning via flow rate control

Active RFQ frequency tuning by employing differential water temperature control within the vane and wall passages has gained widespread acceptance [30,31]. This approach involves precise regulation of the differential water temperature by adjusting the flow speed of the cooling water. Given that (i) all the rf power consumption is absorbed by the cooling water; (ii) the heat transfer is a proximate steady-state process; and (iii) the temperature of the cooling water T_w is consistent inside the RFQ cavity. The steady-state equilibrium equation for the heat transferring can be expressed as

$$hS(T_c - T_w) = vsC_p(T_w - T_0). \tag{5}$$

The left side of Eq. (5) represents the energy transferring from the cavity to the cooling water, where S represents the total surface area of the water pipes, T_c is the temperature of the cavity interface, T_w is the temperature of the cooling water, and h is the heat convection coefficient, which can be estimated by the empirical formulas:

$$h = \frac{N_u K}{d_p}, \tag{6}$$

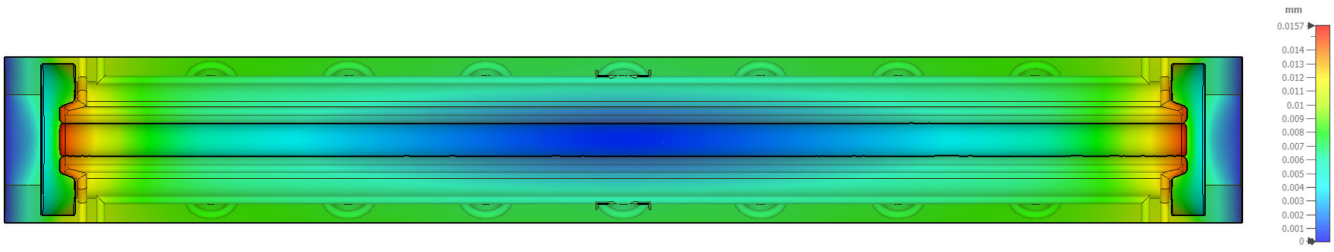

FIG. 12. Thermal deformation of the 704.4 MHz RFQ cavity caused by the temperature rise, when the rf power consumption is 32.3 kW, the cooling water speed is 2 m/s.

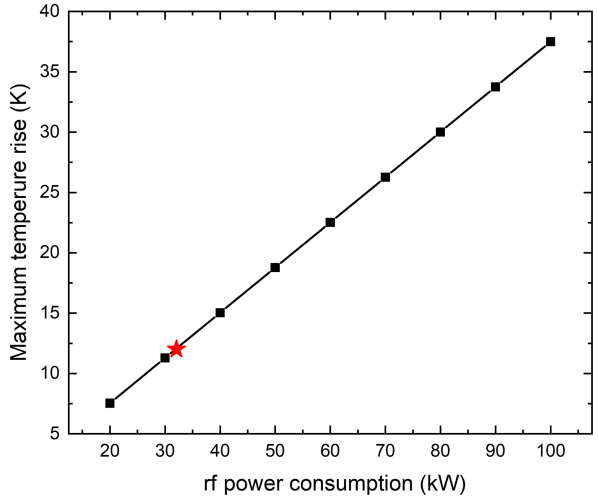

FIG. 13. Maximum temperature rises under different rf power consumption of the FJ RFQ. The red star indicates the temperature rise at 32.3 kW.

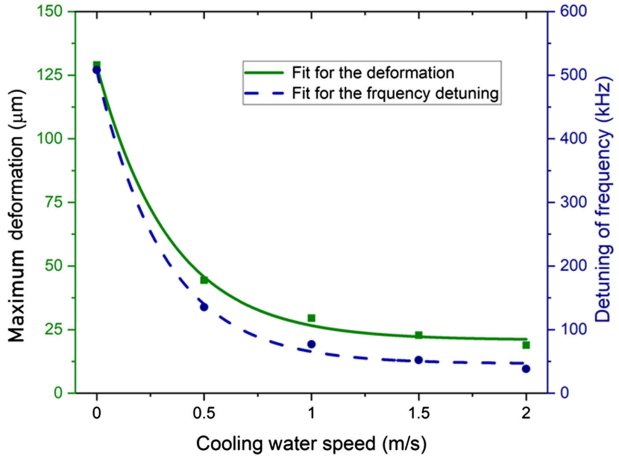

FIG. 14. RFQ deformation and the detuning of frequency under different cooling water speeds.

where K represents the thermal conductivity of the coolant, d_p is the inner diameter of the pipe, and N_u is the Nusselt number. The Nusselt number $N_u \approx 0.023 R_e^{0.8} P_r^{0.4}$, where P_r is the Prandtl number, and R_e is the Reynolds number. The Reynolds number is a very important quantity to predict fluid flow patterns in different situations by measuring the ratio between inertial and viscous forces, which is defined as

$$R_e = \frac{\rho v d_p}{\mu}, \tag{7}$$

where ρ is the fluid density, v is the flow speed, and μ is the dynamic viscosity of the fluid.

The right side of Eq. (5) represents the energy inducing the water temperature rise, where s represents the cross-sectional area of all water pipes, C_p is the specific heat capacity of water, and T_0 is the ambient temperature. Given that the temperature difference between the copper and water $T_c - T_w$ is much higher than the water temperature rises $T_w - T_0$, the steady-state water temperature can be expressed in terms of v as

$$T_w \approx k v^{-0.2} (T_c - T_0) + T_0, \tag{8}$$

where the coefficient k $(= 0.023 \rho^{0.8} P_r^{0.4} K S / d_p^{0.2} \mu^{0.8} C_p s)$ is approximated to be a constant only related to the coolant properties. It can be concluded from Eq. (8) that the steady-state temperature of the cooling water T_w is inversely proportional to $v^{0.2}$, which means that the cooling water with higher velocity could lower the temperature rise more efficiently, as well as the RFQ cavity deformation and the detuning of frequency. It suggests that monitoring the water flow speed provides a direct approach to frequency tuning.

As well known, the turbulent flow is more efficient for cooling than the laminar flow, so it is important to make sure the Reynolds number is larger than 4000 [32]. Given the parameters that the pipe diameter $d_p = 0.01$ m, the water density $\rho \approx 10^3$ kg/m^3, and viscosity $\mu \approx 10^{-3}$ pa·s at atmosphere environment, it is estimated that the velocity of the cooling water v should exceed 0.4 m/s. On the downside, with the increment of water speed, the corrosion of copper would also speed up. When the water speed is 2 m/s around 300 K, the copper corrosion is less than 0.1 mm per year [33,34]. Since the minimum copper wall thickness is more than 2 mm, it is estimated that the FJ RFQ lifetime is at least 20 years without water leakage risks when the water speed is less than 2 m/s.

For the sake of speeding up the simulation time, the pumping ports and the power coupler are replaced by identical tuners, rendering the RFQ structure symmetric in all three dimensions. Figure 14 presents the maximum deformation size and the frequency detuning of the FJ RFQ at various water speeds. The result demonstrates that both deformation and frequency detuning decrease as water speed increases. After the water speed surpasses 1.5 m/s, the changes in the cavity deformation and the detuning frequency become very limited. From Fig. 14, we can conclude that increasing the water speed from 0.4 to 2 m/s would result in a frequency tuning range of about 100 kHz. As the water speed ranges from 1 to 2 m/s, the frequency detuning changes from 78 to 38 kHz. Since the TE_{210} mode frequency is designed as 703.34 MHz, in high power operation the RFQ will operate at 704.4 ± 0.02 MHz with $v = 1$–2 m/s cooling water. The information helps optimize the RFQ performance and fine-tune the frequency through controlled adjustments in the cooling water flow.

IV. CONCLUSIONS AND OUTLOOK

The rf structure including new style water-cooling channels of a 704.4 MHz, $\beta \approx 0.2$, continuous-wave RFQ has been carefully designed and analyzed. Due to

the unique structure of the FJ RFQ with compact transverse cavity dimensions but a large vane size, the AM technology is a promising choice for the construction of the RFQ cavity. In the rf design, an optimized circularlike quadrant structure has been adopted to improve the shunt impedance by $> 7.0\%$. The TE_{210} mode is designed at 704.34 MHz without high power dissipation and the desired frequency can be reached by adjusting 16 tuners with a tuning rate of about 1 MHz/mm. The mode spectrum shows that frequency gaps between the operating mode and its adjacent modes are more than 10 MHz. The field flatness is optimized within $\pm 2\%$ with dedicated undercuts.

Furthermore, the thermal stability has been investigated carefully due to the required cw operation for the FJ RFQ. The AM technology enables the fabrication of curved water-cooling channels around critical undercut areas and insert components. These unconventional cooling channels exhibit excellent heat dissipation capabilities when the cooling water is 2 m/s, the maximum temperature rise is only 12 K and the maximum structure deformation is 15.7 μm. Even if the power consumption is increased to be much higher than the nominal value, the FJ RFQ can still easily avoid overheating. In addition, the multiphysics simulations reveal that by adjusting the cooling water flow from 0.4 m/s to a higher speed, a substantial frequency tuning range of 100 kHz can be achieved. When the cooling water speed ranges from 1 to 2 m/s, the FJ RFQ will operate at 704.4 ± 0.02 MHz.

This study has verified the adaptability and reliability of the 704.4 MHz cw RFQ to be used for the frequency jump at $\beta \approx 0.2$, which can contribute to shortening the whole length and saving the total cost of large-scale hardon linac facilities considerably. Further studies including the dedicated engineering drawings, the AM-based manufacturing, and rf measurements of the FJ RFQ prototype are in arrangement.

ACKNOWLEDGMENTS

The author Bowen Zhou wishes to acknowledge the financial support from the "China and Germany Postdoctoral Exchange Program," Grant No. ZD202118.

[1] R. W. Garnett, LANSCE accelerator update and future plans, J. Phys. Conf. Ser. **1021**, 012001 (2018).

[2] N. Holtkamp *et al.*, Status of the SNS linac: An overview, in *Proceedings of LINAC 2004, Lübeck, Germany* (JACoW, Geneva, Switzerland, 2004).

[3] Y. Liu, Z. Fang, K. Futatsukawa, T. Ito, A. Miura, T. Miyao, T. Morishita, K. Moriya, K. Okabe, M. Otani *et al.*, Progress of J-PARC linac commissioning, in *Proceedings of the 10th International Particle Accelerator Conference, IPAC2019, Melbourne, Australia* (JACoW, CERN, Geneva, Switzerland, 2019).

[4] I. D. Kittelmann, F. Alves, E. Bergman, C. Derrez, V. Grishin, T. Grandsaert, T. Shea, and L. ESS ERIC, Ionisation chamber based beam loss monitoring system for the ESS linac, in *Proceedings of the 8th International Beam Instruments Conference, IBIC2019, Malmö, Sweden* (JACoW, CERN, Geneva, Switzerland, 2019).

[5] D. Vandeplassche, J.-L. Biarrotte, H. Klein, and H. Podlech, The MYRRHA linear accelerator, in *Proceedings of the International Particle Accelerator Conference, IPAC2011, San Sebastian, Spain* (JACoW, Geneva, Switzerland, 2011), WEPS090, pp. 2718–2720.

[6] C. Zhang, D. Koser, N. Petry, H. Podlech, and E. Tanke, Frequency jump using 704.4 MHz radio-frequency quadrupole and cross-bar H-type drift tube linear accelerators, Phys. Rev. Accel. Beams **24**, 040101 (2021).

[7] M. Heilmann, C. Zhang, and H. Podlech, R&D for the realization of a very high frequency crossbar H-mode drift tube linac, in *Proceedings of the 31st International Linear Accelerator Conference, GSI-2023-00477, Strahlkühlung* (JACoW, Geneva, Switzerland, 2022), TUPOJO04.

[8] C. Zhang, M. Heilmann, A. Japs, C. Will, and H. Podlech, Development of a 704.4 MHz CH cavity using additive manufacturing, in *Proceedings of the 14th International Particle Accelerator Conference, IPAC23, Venice, Italy* (JACoW, Geneva, Switzerland, 2023).

[9] S. Jenzer, M. Alves, S. Bilgen, J. Bonis, F. Brisset, S. Djelali, A. Gonnin, M. Guerrier, D. Grasset, F. Letellier-Cohen *et al.*, Is it possible to use additive manufacturing for accelerator UHV beam pipes?, J. Phys. Conf. Ser. **1350**, 012199 (2019).

[10] T. Torims, G. Pikurs, S. Gruber, M. Vretenar, A. Ratkus, M. Vedani, E. López, and F. Brückner, First proof-of-concept prototype of an additive manufactured radio frequency quadrupole, Instruments **5**, 35 (2021).

[11] T. Torims, A. Cherif, N. Delerue, M. F. Pedretti, D. Krogere, T. Otto, G. Pikurs, M. Pozzi, A. Ratkus, M. Thielmann *et al.*, Evaluation of geometrical precision and surface roughness quality for the additively manufactured radio frequency quadrupole prototype, J. Phys. Conf. Ser. **2420**, 012089 (2023).

[12] H. Hähnel and U. Ratzinger, First 3D printed IH-type linac structure proof-of-concept for additive manufacturing of linac rf cavities, Instruments **6**, 9 (2022).

[13] H. Hähnel, A. Ateş, B. Dedić, and U. Ratzinger, Additive manufacturing of an IH-type linac structure from stainless steel and pure copper, Instruments **7**, 22 (2023).

[14] A. Riensche, P. Carriere, Z. Smoqi, A. Menendez, P. Frigola, S. Kutsaev, A. Araujo, N. G. Matavalam, and P. Rao, Application of hybrid laser powder bed fusion additive manufacturing to microwave radio frequency quarter wave cavity resonators, Int. J. Adv. Manuf. Technol. **124**, 619 (2023).

[15] M. Vretenar, E. Montesinos, M. Timmins, M. Garlaschè, A. Grudiev, A. Dallocchio, S. Mathot, V. Dimov, and A. Lombardi, A compact high-frequency RFQ for medical applications, CERN, Geneva, Switzerland, Technical Report No. CERN-ACC-2014-365, 2014.

[16] A. Lombardi, E. Montesinos, M. Timmins, M. Garlaschè, A. Grudiev, S. Mathot, V. Dimov, S. Myers, and M. Vretenar, Beam dynamics in a high frequency RFQ, in

Proceedings of the 6th International Particle Accelerator Conference, IPAC2015, Richmond, VA (JACoW, CERN, Geneva, Switzerland, 2015).

[17] M. Vretenar, V. Dimov, M. Garlaschè, A. Grudiev, B. Koubek, A. Lombardi, S. Mathot, D. Mazur, E. Montesinos, M. Timmins *et al.*, High-frequency compact RFQs for medical and industrial applications, in *Proceedings of the 28th Linear Accelerator Conference, LINAC16, East Lansing, MI* (JACoW, Geneva, Switzerland, 2016), p. 33.

[18] B. Koubek, A. Grudiev, and M. Timmins, rf measurements and tuning of the 750 MHz radio frequency quadrupole, Phys. Rev. Accel. Beams **20**, 080102 (2017).

[19] H. Pommerenke, A. Bilton, A. Grudiev, A. Lombardi, S. Mathot, E. Montesinos, M. Timmins, M. Vretenar, U. van Rienen *et al.*, rf design of a high-frequency RFQ linac for PIXE analysis, in *Proceedings of the 29th Linear Accelerator Conference, LINAC18, Beijing, China* (JACoW, Geneva, Switzerland, 2018), pp. 822–825.

[20] H. W. Pommerenke, V. Bencini, A. Grudiev, A. M. Lombardi, S. Mathot, E. Montesinos, M. Timmins, U. van Rienen, and M. Vretenar, rf design studies on the 750 MHz radio frequency quadrupole linac for proton-induced x-ray emission analysis, Phys. Rev. Accel. Beams **22**, 052003 (2019).

[21] T. P. Wangler, *rf Linear Accelerators* (John Wiley & Sons, Hoboken, NJ, 2008).

[22] C. M. Studio, CST Studio Suite, CST Microwave Studio, 2008.

[23] F. Grespan, A. Pisent, and A. Palmieri, Dipole stabilizers for a four-vane high current RFQ: Theoretical analysis and experimental results on a real-scale model, Nucl. Instrum. Methods Phys. Res., Sect. A **582**, 303 (2007).

[24] H. Podlech, K. Kümpel, C. Lorey, P. Schneider, N. Petry, A. Schempp, C. Zhang, and A. Bechtold, The MYRRHA-RFQ-status and first measurements, in *Proceedings of the International Particle Accelerator Conference, IPAC'17, Copenhagen, Denmark* (JACoW, CERN, Geneva, Switzerland, 2017), pp. 2243–2245.

[25] G. Turemen, B. Yasatekin, S. Ogur, V. Yildiz, O. Mete, S. Oz, A. Ozbey, H. Yildiz, F. Yaman, Y. Akgun *et al.*, Current status of the SANAEM RFQ accelerator beamline, in *Proceedings of the 6th International Particle Accelerator Conference, IPAC2015, Richmond, VA* (JACoW, Geneva, Switzerland, 2015), p. 3952.

[26] D. P. Pritzkau and R. H. Siemann, Experimental study of rf pulsed heating on oxygen free electronic copper, Phys. Rev. Accel. Beams **5**, 112002 (2002).

[27] A. Bejan, *Advanced Engineering Thermodynamics* (John Wiley & Sons, Hoboken, NJ, 2016).

[28] L. Laurent, S. Tantawi, V. Dolgashev, C. Nantista, Y. Higashi, M. Aicheler, S. Heikkinen, and W. Wuensch, Experimental study of rf pulsed heating, Phys. Rev. ST Accel. Beams **14**, 041001 (2011).

[29] V. Lacis, Laser polishing of additively manufactured RFQ prototype, CERN, Geneva, Switzerland, Technical Report No. CERN-STUDENTS-Note-2022-1210, 2022.

[30] S. Virostek, M. Hoff, A. Lambert, D. Li, J. Staples, G. Romanov, and C. Zhang, Design and analysis of the PXIE CW radio-frequency quadrupole (RFQ), in *Proceedings of the 3rd International Particle Accelerator Conference IPAC2012, New Orleans, LA* (CERN, Geneva, Switzerland, 2012), THPPC034.

[31] A. Edelen, S. Biedron, S. Milton, D. Bowring, B. Chase, J. Edelen, and J. Steimel, Neural network model of the PXIE RFQ cooling system and resonant frequency response, in *Proceedings of the 2016 International Particle Accelerator Conference, IPAC'16, Busan, Korea* (CERN, Geneva, Switzerland, 2016), THPOY020.

[32] X. Zhu, C. Marchand, O. Piquet, and M. Desmons, Coupled multiphysics analysis of a 4-vane RFQ accelerator under high power operation, J. Instrum. **17**, P03011 (2022).

[33] R. Francis, *The Corrosion of Copper and Its Alloys: A Practical Guide for Engineers* (NACE International, Houston, TX, 2010).

[34] H. M. Mahmood, S. Suryanto, and M. H. F. Al Hazza, The effects of water flow rate on copper corrosion, Key Eng. Mater. **748**, 235 (2017).